Schizophrenia Bulletin vol. 49 no. 5 pp. 1355–1363, 2023
https://doi.org/10.1093/schbul/sbad041
Advance Access publication April 8, 2023

Quantitative Susceptibility Mapping MRI in Deep-Brain Nuclei in First-Episode Psychosis

Marisleydis García Saborit[1,2,3], Alejandro Jara[4], Néstor Muñoz[1,2,3], Carlos Milovic[5], Angeles Tepper[3,6], Luz María Alliende[6], Carlos Mena[6], Bárbara Iruretagoyena[6], Juan Pablo Ramirez-Mahaluf[6], Camila Diaz[7], Ruben Nachar[7], Carmen Paz Castañeda[7], Alfonso González[8,9], Juan Undurraga[8,10], Nicolas Crossley[2,3,6], and Cristian Tejos[*,1,2,3]

[1]Department of Electrical Engineering, Pontificia Universidad Catolica de Chile, Santiago, Chile; [2]Biomedical Imaging Center, Pontificia Universidad Catolica de Chile, Santiago, Chile; [3]Millennium Institute for Intelligent Healthcare Engineering, Santiago, Chile; [4]Department of Statistics, Mathematics Faculty, Pontificia Universidad Catolica de Chile, Santiago, Chile; [5]School of Electrical Engineering, Pontificia Universidad Catolica de Valparaiso, Valparaiso, Chile; [6]Department of Psychiatry, School of Medicine, Pontificia Universidad Catolica de Chile, Santiago, Chile; [7]Pharmacovigilance, Instituto Psiquiátrico Dr. J. Horwitz Barak, Santiago, Chile; [8]Early Intervention Program, Instituto Psiquiátrico Dr J. Horwitz Barak, Santiago, Chile; [9]School of Medicine, Universidad Finis Terrae, Santiago, Chile; [10]Department of Neurology and Psychiatry, Faculty of Medicine, Clínica Alemana Universidad del Desarrollo, Santiago, Chile

*To whom correspondence should be addressed; Av. Vicuña Mackenna 4860, Chile; tel: +56 9 5504 1280, e-mail: ctejos@uc.cl

***Background*: Psychosis is related to neurochemical changes in deep-brain nuclei, particularly suggesting dopamine dysfunctions. We used an magnetic resonance imaging-based technique called quantitative susceptibility mapping (QSM) to study these regions in psychosis. QSM quantifies magnetic susceptibility in the brain, which is associated with iron concentrations. Since iron is a cofactor in dopamine pathways and co-localizes with inhibitory neurons, differences in QSM could reflect changes in these processes. *Methods*: We scanned 83 patients with first-episode psychosis and 64 healthy subjects. We reassessed 22 patients and 21 control subjects after 3 months. Mean susceptibility was measured in 6 deep-brain nuclei. Using linear mixed models, we analyzed the effect of case-control differences, region, age, gender, volume, framewise displacement (FD), treatment duration, dose, laterality, session, and psychotic symptoms on QSM. *Results*: Patients showed a significant susceptibility reduction in the putamen and globus pallidus externa (GPe). Patients also showed a significant R2* reduction in GPe. Age, gender, FD, session, group, and region are significant predictor variables for QSM. Dose, treatment duration, and volume were not predictor variables of QSM. *Conclusions*: Reduction in QSM and R2* suggests a decreased iron concentration in the GPe of patients. Susceptibility reduction in putamen cannot be associated with iron changes. Since changes observed in putamen and GPe were not associated with symptoms, dose, and treatment duration, we hypothesize that susceptibility may be a trait marker rather than a state marker, but this must be verified with long-term studies.**

Key words: QSM/magnetic susceptibility/dopamine/neuromelanin/R2* rates

Introduction

Psychosis is associated with neurochemical changes in the brain that are the target of existing pharmacological treatments as well as the focus for the development of future therapies. Several lines of evidence suggest that psychosis is associated with abnormalities in deep-brain nuclei, particularly the striatum, and is linked to dopamine dysfunction.[1–3] Characterization of the neurochemical changes in these regions rich with neuro-modulatory activity could provide clinically relevant information for the management of patients with psychosis and contribute to our understanding of the pathophysiology of psychosis, particularly schizophrenia.

One of the challenges facing neuroimaging-based assessment of neuro-modulatory systems of deep-brain nuclei, such as dopaminergic functioning in patients, is that it is mostly based on Positron Emission Tomography (PET) imaging. Magnetic Resonance Imaging (MRI)-based techniques that could inform this problem might become an attractive alternative in terms of cost, safety, and availability. Several studies have used MRI spectroscopy to characterize the neurochemical properties of different deep-brain nuclei.[4,5] Recent studies have shown that 2 other modalities could contribute to this goal: Neuromelanin-Sensitive MRI (NM-MRI) and Quantitative Susceptibility Mapping

(QSM). NM-MRI, combines Magnetization Transfer and Longitudinal Relaxation contrasts mechanisms to detect neuromelanin[6] and it has been suggested as a noninvasive proxy measure of dopamine function in the human brain.[7] Neuromelanin is a byproduct of the metabolism of dopamine and an effective iron chelator, thus protecting neurons from oxidative stress. Neuromelanin is found in iron-rich areas such as substantia nigra pars compacta and locus coeruleus.[5,7] NM-MRI signal in the substantia nigra has been shown as abnormal in patients with Parkinson's disease,[5,8] and those at higher risk of developing psychosis.[9,10] Recently, it has been suggested that increased NM levels in the substantia nigra (SN) may be a potential biomarker for stratifying schizophrenia.[11]

QSM allows measuring changes in the magnetic susceptibility of brain tissues,[12] usually produced by changes in myelin structure or in the concentration of chemical species such as iron.[13–15] This factor is particularly interesting since deep-brain nuclei, such as the SN, are particularly rich in iron and have a strong susceptibility. An in-vivo window into brain iron status would certainly be informative. Iron is fundamental for many brain processes such as oxygen transportation and energy metabolism, DNA synthesis, neuronal development, myelin production, as well as maintaining the integrity of neurochemical circuits such as the monoaminergic, glutamatergic, and the gamma aminobutyric acid (GABA) system.[16–20] Iron has also been linked to inhibitory synapses.[21] Consequently, the dysregulation of iron homeostasis has been implicated in various neuropsychiatric disorders.[18,22]

QSM has been validated in postmortem studies and used to characterize iron changes in multiple sclerosis, Parkinson's, and Huntington's disease.[13,23,24] Iron deficiency in first-episode schizophrenia (measured in the peripheral blood) has been associated with more severe negative symptoms.[25] Localized changes of iron concentration in basal ganglia have been also associated with motor abnormalities[26] in schizophrenia. Localized iron measurements may highlight some specific mechanisms associated with psychosis. Iron could indirectly reflect the dopaminergic tone in the brain since it binds to neuromelanin, providing similar information to neuromelanin-based MRI. On the other hand, ferritin-bound iron, which is the major contributor to the paramagnetism observed in gray matter,[27] is particularly rich in oligodendrocytes and is essential in myelin formation.[28] As such, QSM maps are expected to differ to some extent from the neuromelanin-based approaches, providing complementary information. A recent study[20] recruited 35 first episode psychosis (FEP) patients and found significant QSM differences (less paramagnetic values) in the bilateral substantia nigra, left red nucleus, and left thalamus, when compared to healthy controls.

We here explored the use of QSM in 83 subjects with FEP, comparing it with 64 healthy controls. We first explored potential susceptibility differences between the 2 groups in deep-brain nuclei. QSM measurements were also complemented with R2* measurements to confirm the presence of paramagnetic elements (eg, iron).[13,27] In line with Xu et al.,[20] we hypothesized that using QSM we would find decreased susceptibilities in the striatum, which would be also in line with the opposite finding in hypo-dopaminergic states such as Parkinson's.[29] We then examined whether QSM was related to symptom levels in patients with psychosis, as has been previously shown with NM-MRI.[7] We also performed a second MRI scan and reassessed 22 patients (after treatment of their first episode) and 21 controls obtained 3 months after their baseline.

Methods

Participants

We invited patients between 15 and 27 years of age with a first episode of nonaffective psychosis admitted to the ward from the Early Intervention in Psychosis Program of the Instituto Psiquiátrico Dr. J Horwitz in Santiago, Chile. All subjects fulfilled the criteria for a first-psychotic disorder according to the Mini International Neuropsychiatric Interview (MINI[30]), were in their first presentation to mental health services, and were receiving treatment according to local guidelines, including antipsychotic medication.[31] Patients with major medical or neurological comorbidities were excluded. We also recruited healthy control subjects without any current psychiatric disorder or lifetime history of psychotic disorder, according to the MINI. A subgroup of participants from both groups was invited to a new assessment and scan approximately 3 months after their first MRI scan. Any subject with metallic or electronic implants, metallic foreign objects, or severe claustrophobia was also excluded. We analyzed potential demographic differences between patients and controls using a Mann-Whitney *U* test.

All subjects gave their written consent to participate in the study (or assent if under 18 alongside their guardians' consent). This project was approved by the ethics committee of the Pontificia Universidad Católica de Chile and the Northern Metropolitan Health Service.

Clinical Assessment

Patients were assessed by 2 psychiatrists experienced in psychotic disorders and clinical treatments were prescribed following the Chilean guidelines for first-episode schizophrenia.[31] Semi-structured interviews with patients and family members, medical records, and systematic follow-up assessments provided socio-demographic data and clinical details of illness history. In addition, patients were assessed using the Positive and Negative Syndrome Scale (PANSS)[32] at baseline and at 3 months follow-up (if rescanned).

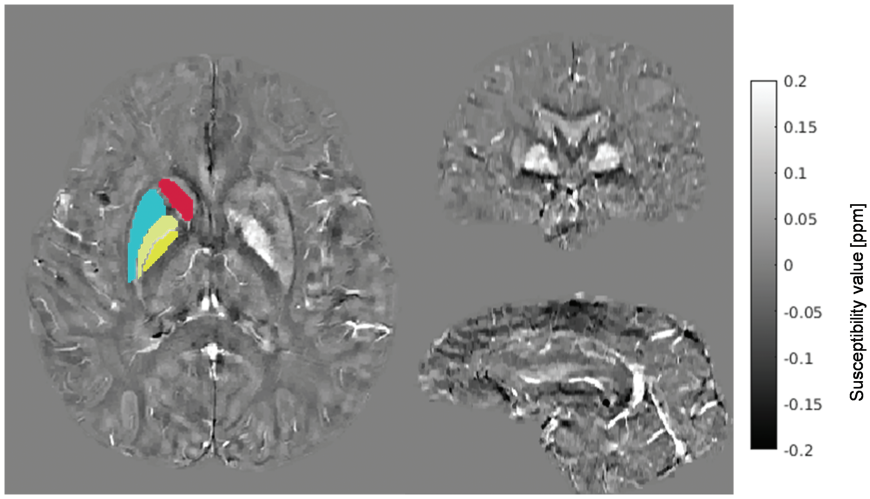

Fig. 1. Axial, sagittal, and coronal slice of a reconstructed QSM map showing Caudate (red), Putamen (blue), Globus Pallidus externa (GPe), and Globus Pallidus interna (GPi), both in yellow.

Image Acquisition and Normalization

Subjects were scanned in a 3T Philips Ingenia MRI scanner. QSM maps and R2* rates were obtained using a 3D Turbo Gradient Echo sequence, voxel size = 0.59 × 0.59 × 1 mm^3, TR/TE/ΔTE = 4/7.2/6.2 ms, 5 echoes, bandwidth = 550.5 Hz, matrix size = 352 × 352 × 160, flip angle = 17°. QSM and R2* images were co-registered to a structural T1 weighted image with the following parameters: voxel size = 0.5 × 0.5 × 1 mm^3, TR/TE = 7.75/3.57 ms, bandwidth = 191.0 Hz, matrix size = 480 × 480 × 341, and flip angle = 8°. The co-registered QSM and R2* images were normalized in the MNI space using SPM12 (https://www.fil.ion.ucl.ac.uk/spm/software/spm12/) and a third-order B-spline interpolation. We also acquired resting-state functional MRI (fMRI) scans collected with a single-shot full k-space echo-planar imaging (voxel size = 2.75 × 2.75 × 3 mm^3, TR/TE = 2499.9/35 ms, bandwidth = 2054.0 Hz, matrix size = 80 × 80, flip angle = 82°). We used framewise displacement (FD)[33,34] computed from the fMRI images to assess head motion during the scanning session and to control for movement in our statistical analyses of QSM data.

QSM Reconstruction

QSM reconstructions were obtained from the phase of the gradient-echo MRI acquisitions following a 3-step pipeline. First, 2π-jumps in the phase signal were removed by a Laplacian unwrapping operator.[35] Second, phase contributions from objects outside the region of interest (ROI) and field inhomogeneities were removed after the application of a background field removal process. This process included three consecutive subprocesses: a Laplacian Boundary Value,[36] a polynomial fit subtraction (function implemented in the FAst Nonlinear Susceptibility Inversion (FANSI) toolbox (https://gitlab.com/cmilovic/FANSI-toolbox), and Variable Sophisticated Harmonic Artifact Reduction for Phase data.[37] Third, the final susceptibility distribution was obtained from the phase signal obtained in the previous step using FANSI algorithm,[38] Weak Harmonic QSM (WH-QSM),[39] and a Total Variation regularizer,[40] all included in the FANSI toolbox. The optimal parameters for the third step were chosen following an L-curve procedure[41] (L = 20). Those parameters included: regularization weight $\alpha = 1 \times 10^{-4}$, harmonic consistency weight $\mu = 0.1$, maximum number of iterations = 300, convergence parameter = 0.1, gradient consistency weight $\mu_1 = 0.01$, fidelity consistency weight $\mu_2 = 1.0$, and harmonic constraint weight $\beta = 50$. An example of a reconstructed QSM image can be seen in figure 1, highlighting the contrast in basal ganglia.

A rise in the bulk susceptibility within a voxel could be explained by 2 phenomena, an increment of paramagnetic substances (eg, iron) or a reduction of diamagnetic substances (eg, calcium). Such ambiguity can be solved by jointly analyzing QSM maps and R2* rates, since both paramagnetic and diamagnetic concentrations are proportional to R2* values.[13,27] Therefore, we also reconstructed R2* rates (from the same gradient echo acquisitions used for QSM) to explain potential brain nuclei changes. R2* maps were reconstructed using a nonlinear method available in the FANSI toolbox.

Region of Interest Analysis

ROIs were segmented using the Multicontrast PD25 atlas.[42–44] Given their relationship with dopamine, we defined the following 6 subcortical structures to explore: Substantia nigra (SN), Caudate, Putamen, Globus Pallidus externa (GPe), Globus Pallidus interna (GPi), and Thalamus. For each ROI, we considered the mean susceptibility value.

Table 1. Clinical and Demographic Data of the Studied Cohort (At Times t_1 and t_2)

Variable	Control Subjects t_1	Patients t_1	*P*-Value	Control Subjects t_2	Patients t_2	*P*-Value
Sample size	64	83	Not applicable	21	22	Not applicable
Age*—mean (range)	23 (15–32)	20 (15–27)	<.001	24 (16–32)	20 (16–24)	.0013
Gender—*N* (% women)	25 (39)	20 (24)	.052	8 (38)	6 (27)	.353
Movement within the scanner (measured by the FD)—mean (range)	0.32 (0–0.72)	0.42 (0.16–3.59)	.057	0.44 (1.49–0.17)	0.34 (0–0.96)	.641
Interval between scans (days)—mean (range)	0	0	Not applicable	128 (75–309)	118 (75–252)	.183
	Patients t_1	**Patients t_2**				
Total Positive (PANSS) —mean (range)	16 (9–43)	12 (7–28)				
Total Negative (PANSS) —mean (range)	20 (7–46)	15 (7–39)				
Total General (PANSS) —mean (range)	32 (16–75)	24 (15–46)				
Total PANSS—mean (range)	67 (39–158)	50 (30–108)				
Medication dose (in chlorpromazine equivalents)—mean (range)	494 (25–1200)	518 (100–900)				
Days of treatment—mean (range)	25 (0–140)	142 (75–261)				

*Significant differences between patients and controls were found only for the variable mean age (according to a Mann–Whitney *U* test).

Table 2. Marginal *F* Statistic and Corresponding *P*-Value for the Selected Factors for QSM/R2* Via a Backward Selection Procedure and a Random Intercept Model

Factor	*F*	*P*-Value
QSM		
Region	42.916	<.001
Age	3.935	.049
Region × Gender	2.635	.015
Region × Group	5.022	<.001
R2*		
Region	65.518	<.001
Group	65.518	.015
Age	6.046	<.001
Region × Group	35.18	<.001

Statistical Analysis

We evaluated the effect of predictors on the susceptibility and R2* rates at the first scan (t_1), including group, region, age, gender, laterality, volume, dose, total general PANSS score, days of treatment, and FD as predictors. We used linear mixed models[45] to take into account the correlation of the measurements of the same subjects. We focused on measurements at t_1 since only a reduced number of patients (22 individuals) were reevaluated at t_2, and, more importantly, patients have a shorter treatment window at t_1. We thus tried to eliminate from the analyses the confounding factor given by treatment time. Starting with a model including all interactions, we performed a backward elimination procedure based on the *P*-value associated with the *F*-statistics of the marginal Wald test for the terms in each random intercept model.[46] In the marginal Wald test, the sum of squares is obtained by deleting one term from the model at a time and computing the reduction in the sum of squares. To evaluate the robustness of the inferences to the implied correlation assumption under the random intercept model,[47] inferences on the coefficients under a semiparametric marginal model fit using Generalized Estimating Equations (GEE)[48] are also provided. We considered significantly different *P*-values of less than .05. All statistical analyzes were performed using "nlme"[46] and "geepack"[49] packages in R version 4.2.0.

As described in the Methods, R2* rates provide additional information and can help in the interpretation of changes observed in QSM (differentiating signal changes due to increased or decreased paramagnetic or diamagnetic substances). We also analyzed potential correlations between QSM and R2* in each ROI.

Results

Dataset Characteristics

Initially, 95 patients and 68 controls were considered in our study. We excluded 12 patients and 4 control subjects since QSM-MR scans presented severe image artifacts, particularly motion, leading to a final sample of 83 patients and 64 healthy controls. Characteristics of the included patients and controls are summarized in table 1. Both groups were comparable at baseline (time t_1) and only showed a significant difference in mean age (20 vs 23 years), which was controlled for in subsequent analyses. After 3 months, we assessed a subgroup of 22 patients and 21 control subjects as previously described.

*Case-Control Differences in QSM and R2**

Region, age, gender, and group were significant variables for QSM, while region, age, and group were significant variables for R2*. Table 2 shows the test statistics for the selected factors under the random intercept model for QSM and R2* in the first session. A significant interaction between region and group was observed for QSM

Table 3. Estimate, Standard Error (Std. Error), and *P*-Value for the Regression Coefficients Under the Random Intercept Model for QSM

	Random intercept model			Marginal model		
Coefficient	Estimate	Std. Error	*P*-Value	Estimate	Std. Error	*P*-Value
(Intercept)	0.006	0.011	.605	0.006	0.007	.427
Putamen	−0.012	0.004	**.004**	−0.012	0.005	**.021**
Caudate	−0.022	0.004	**<.001**	−0.022	0.005	**<.001**
GPe	0.022	0.004	**<.001**	0.022	0.006	**<.001**
GPi	0.012	0.004	**.005**	0.012	0.008	.125
Thalamus	−0.029	0.004	**<.001**	−0.029	0.005	**<.001**
Age	0.001	0.0005	**.049**	0.001	0.0003	**.001**
Substantia nigra × Gender 1	−0.004	0.005	.383	−0.004	0.006	.517
Putamen × Gender 1	−0.002	0.005	.624	−0.002	0.001	.078
Caudate × Gender 1	−0.002	0.005	.606	−0.002	0.001	**.002**
GPe × Gender 1	−0.007	0.005	.151	−0.007	0.004	.069
GPi × Gender 1	0.013	0.005	**.006**	0.013	0.007	.066
Thalamus × Gender 1	−0.002	0.005	.672	−0.002	0.001	**.029**
Substantia nigra × Group 1	−0.0004	0.004	.933	−0.0004	0.006	.947
Putamen × Group 1	−0.002	0.004	.738	−0.002	0.001	.302
Caudate × Group 1	−0.002	0.004	.64	−0.002	0.001	.057
GPe × Group 1	−0.021	0.004	**<.001**	−0.021	0.004	**<.001**
GPi × Group 1	−0.001	0.004	.803	−0.001	0.007	.865
Thalamus × Group 1	0.001	0.004	.809	0.001	0.001	.378

Bold indicate statistical significant was set for $P < .05$.

Table 4. Estimate and *P*-value for the Region-Specific Regression Coefficient of the Group Treatment Effect Under the Random Intercept model for QSM and R2*

Area	**Estimate**	***P*-value**	**Estimate**	***P*-value**
	QSM		R2*	
Substantia nigra	0.004	.635	−0.002	.138
Caudate	−0.001	.395	−0.001	.056
Putamen	−0.003	**.004**	−0.0002	.566
Globus Pallidus externa	−0.021	**<.001**	**−0.002**	**.037**
Globus Pallidus interna	−0.002	.86	0.001	.418
Thalamus	−0.001	.061	−0.0002	.665

Bold indicate statistical significant was set for $P < .05$.

and R2*, implicating the existence of region-specific differences in QSM and R2* between controls and patients.

The intra-class correlation under the conditional model was 0.1820 and 0.1602 for QSM and R2*, respectively. Table 3 shows the inferences on the coefficients under the random intercept model, along with the coefficients under a semiparametric marginal model which regression coefficients are estimated using GEE. The results show that the inferences on the regression coefficients are robust to the association structure implied by the assumed random intercept model. Supplementary table S1 reported the coefficients for R2*.

To understand the effect modifier effect of the region, stratified analyses by treatment group were performed. Table 4 shows the effect of the patients for each region and the corresponding *P*-value. The results suggest that patients with first-episode psychosis have a significantly lower QSM in the putamen and GPe (supplementary figure S2). And R2* rates only showed lower values in GPe (supplementary figure S3). No significant differences were found in the other regions. Supplementary figure S1 showed a deep-brain nuclei of controls hyperintense QSM maps compared with patients.

*Correlation Between QSM and R2**

Considering patients and controls as a single group at time t_1, Pearson's analysis reported significant correlations between susceptibility and R2* in 2 areas: SN (rho = 0.133 and $P = .03$) and globus pallidus externa (rho = 0.143 and $P = .019$) (supplementary table S2). Interestingly, when only patients are analyzed at t_1, these areas showed no correlation between QSM and R2*, and those significant correlations changed to be at the caudate, putamen, GPi, and thalamus. When only controls were analyzed at t_1, all areas showed correlations between QSM and R2* except SN. Finally, when only patients are analyzed but at t_2, areas showing correlations were the caudate, putamen, and thalamus (supplementary table S2). In supplementary table S3, we reported mean QSM and R2* rates for each ROI, and in supplementary table S4 mean of volume.

Discussion

QSM is a novel MRI-based approach that could provide new insights about the neural underpinnings of psychosis by looking at iron concentrations in the brain.

Iron-bounded compounds are linked to multiple processes in the brain, including dopamine metabolism, GABA systems, among other mechanisms involved in psychosis.[50]

QSM measures bulk susceptibility. This means that, within a voxel, any chemical species causing a susceptibility change will contribute to some extent to the measured value. R2* maps in conjunction with QSM maps could differentiate between diamagnetic (eg, calcium) and paramagnetic (eg, iron) sources.[13,27] Using QSM, various sources of iron found in the brain (eg, ferritin-bounded, neuromelanin-bounded) are measured together, unfortunately without any differentiation. Although some efforts have been made to discriminate among those different sources of iron, standard QSM strategies cannot provide such a result and further research work is needed in this area.

As we initially hypothesized, there were striatal differences between groups in QSM, particularly in the putamen. This result adds to the evidence provided with PET scans showing striatum abnormalities in psychosis, including striatal differences in dopaminergic tone, particularly in the dorsal striatum,[51] as well as abnormal putaminal-cortical connectivity.[52] The striatum is related to several neurotransmitter systems affected in schizophrenia, such as dopamine, glutamate, and serotonin.[53] These mechanisms do not have a direct relationship with abnormal iron metabolism in psychosis. Accordingly, the exact mechanisms causing the QSM differences are still uncertain. The putamen is a region innervated by dopaminergic neurons, and iron (modifying the QSM) is a co-factor of multiple steps in mono-amine metabolism, including its chelation into neuromelanin in this region.[54] As such, changes in iron concentration may be reflecting changes in the dopaminergic tone.

When analyzing the GPe of FEP patients, we found a decrease in both QSM and R2* values. This finding indicates a reduction of paramagnetic elements, particularly iron. An earlier study[55] found a proliferation of axon terminals to their normal levels in the GPe in an animal model of schizophrenia. Iron has been linked not only to myelin formation processes but also to transport processes near axon terminals that have a substantial turnover of myelin.[56,57]

Patients also showed a susceptibility reduction in the putamen. Here R2* rates did not show a significant change and therefore introduced another viewpoint. It is unclear whether iron depositions decrease or diamagnetic substances increase in this area. Although QSM and R2* are somehow correlated (as we verified in our experiments), they can produce different statistical results. Similarly, a previous study found that QSM and R2* values reported different areas with significant differences.[58] The authors proposed using the Iron Microstructure Coefficient (IMC) to analyze brain tissue magnetic susceptibility and R2* maps simultaneously. In some areas, IMC was significantly different compared to R2* maps. Since the decrease in susceptibility at the putamen cannot be entirely explained by a reduction of iron, we might consider that changes in diamagnetic structures could also be involved (eg, myelin).

Quantitatively, our QSM values are lower than those reported by Xu et al.[20] Qualitatively, they reported susceptibility differences in substantial nigra, left red nucleus, and left thalamus, differences that we only found in the GPe and putamen. These differences could be explained by the fact that different processing pipelines might produce some differences in the quantified susceptibility or by some statistical differences of their smaller cohort. Studies combining PET with QSM, or combining NM-MRI with QSM, postmortem tissue, pharmacological challenges, as well as studies in animal models could provide further insights about these differences. Studying SN with NM-MRI, Ueno et al.[11] reported higher Neuromelanin levels in schizophrenia compared with controls. If in SN the only source of iron was that bound to Neuromelanin, schizophrenia patients should show an increased susceptibility. Other chemical species (particularly other iron sources) affecting susceptibility might be involved in SN; however, considering the relationship of Neuromelanin-bonded iron vs susceptibility (QSM), the results in[11] and those showing a decreased susceptibility in[20] might be counterintuitive.

Our QSM results showed larger intra and interindividual variability compared to those in.[11] This result may be an effect of a small misclassification of our automatic segmentation process based on the use of an atlas. Importantly, our QSM reconstruction process was designed to avoid over-smoothed results, which is a common accuracy problem of current QSM reconstruction algorithms.[59] Changes in QSM were not associated with nuclei volumes; therefore, potential dependencies with atrophy might be ruled out. However, the susceptibility variability depends on region, group, gender, and age. Therefore, all these predictor variables have been considered to study the characteristics of patients.

Since susceptibility changes observed in putamen and GPe were not associated with psychotic symptoms, dose, and treatment duration, we hypothesize that susceptibility may be a trait marker rather than a state marker, but this must be verified with long-term studies.

Our study has several limitations. QSM might be affected by motion. We here managed this by excluding a number of subjects whose images were corrupted by movement. Additionally, in our statistical model, we included a measure of movement in the scanner (FD). Our control subjects were slightly older than our patients, and it is known that QSM increases with age in some brain areas, particularly in the caudate, putamen, and substantia nigra.[14,60,61] To account for this difference, we included a variable *age* in our statistical analyses. We also found an age-related effect in QSM. QSM

might be affected by microvascular blood flow, blood pressure,[62] and demyelination[13] in the ROIs, however we did not control for these confounding effects. Another limitation in our longitudinal study is the rather small number of subjects included for the second MRI scan and the time interval between scans is also small. A larger group rescanned in a longer time window might better capture the response to pharmacological treatment and eventual changes in susceptibilities or iron concentrations.

Other nuclei are also of interest for future studies. For example, the pallidus has also been previously involved in schizophrenia, with studies showing an abnormal structure[63,64] as well as function.[65] This region is known to be rich in iron[66,67] and consequently has a strong signal in QSM images (figure 1). Iron in this region could be associated with its multiple inhibitory neurons and synapses, but also to dopaminergic pathways previously examined with PET. Interestingly, a PET study reported that antipsychotic treatment reduced a radioligand ([11C] PHNO) binding in the caudate/putamen, which mainly represents D2 receptors. In contrast, the same treatment increased a radioligand binding in D3-rich regions, notably in the globus pallidus.[68] However, another theory speculated that dopamine can modulate globus pallidus neuronal activity directly through stimulation of pre and postsynaptic D2 family receptors.[69]

Future studies should also explore QSM changes in a more chronic population and examine the mechanisms responsible for iron differences. This future research could demonstrate QSM as an indirect measurement for analyzing the undergoing neurophysiological processes involved in psychosis and their relationship with iron metabolism.

Supplementary Material

Supplementary material is available at https://academic.oup.com/schizophreniabulletin/.

Acknowledgments

We thank ANID for their grant funding: Fondecyt 1191710, Fondecyt 1200601, Fondecyt 1180358, Fondecyt 1231535, PIA-ACT192064 and PIA-ACT1414 and the Millennium Institute for Intelligent Healthcare Engineering (ICN2021004).

References

1. Howes OD, Kapur S. The dopamine hypothesis of schizophrenia: version III—The final common pathway. *Schizophr Bull.* 2009;35(3):549–562. doi:10.1093/schbul/sbp006.
2. McCutcheon RA, Abi-Dargham A, Howes OD. Schizophrenia, dopamine and the striatum: from biology to symptoms. *Trends Neurosci.* 2019;42(3):205–220. doi:10.1016/j.tins.2018.12.004.
3. Jauhar S, Veronese M, Nour MM, *et al*. The effects of antipsychotic treatment on presynaptic dopamine synthesis capacity in first-episode psychosis: a positron emission tomography study. *Biol Psychiatry.* 2019;85(1):79–87. doi:10.1016/j.biopsych.2018.07.003.
4. Wei H, Frey AM, Jasanoff A. Molecular fMRI of neurochemical signaling. *J Neurosci Methods.* 2021;364:1–11. doi:10.1016/J.JNEUMETH.2021.109372.
5. Zecca L, Shima T, Stroppolo A, *et al*. Interaction of neuromelanin and iron in substantia nigra and other areas of human brain. *Neuroscience.* 1996;73(2):407–415. doi:10.1016/0306-4522(96)00047-4.
6. Trujillo P, Summers PE, Ferrari E, *et al*. Contrast mechanisms associated with neuromelanin-MRI. *Magn Reson Med.* 2017;78(5):1790–1800. doi:10.1002/mrm.26584.
7. Cassidy CM, Zucca FA, Girgis RR, *et al*. Neuromelanin-sensitive MRI as a noninvasive proxy measure of dopamine function in the human brain. *Proc Natl Acad Sci U S A.* 2019;116(11):5108–5117. doi:10.1073/pnas.1807983116.
8. Sulzer D, Cassidy C, Horga G, *et al*. Neuromelanin detection by magnetic resonance imaging (MRI) and its promise as a biomarker for Parkinson's disease. *NPJ Parkinsons Dis.* 2018;4(1):1–13. doi:10.1038/S41531-018-0047-3.
9. Shibata E, Sasaki M, Tohyama K, *et al*. Use of neuromelanin-sensitive mri to distinguish schizophrenic and depressive patients and healthy individuals based on signal alterations in the substantia nigra and locus ceruleus. *Biol Psychiatry.* 2008;64(5):401–406. doi:10.1016/j.biopsych.2008.03.021.
10. Watanabe Y, Tanaka H, Tsukabe A, *et al*. Neuromelanin magnetic resonance imaging reveals increased dopaminergic neuron activity in the substantia nigra of patients with schizophrenia. *PLoS One.* 2014;9(8):1–6. doi:10.1371/journal.pone.0104619.
11. Ueno F, Iwata Y, Nakajima S, *et al*. Neuromelanin accumulation in patients with schizophrenia: A systematic review and meta-analysis. *Neurosci Biobehav Rev.* 2022;132:1205–1213. doi:10.1016/J.NEUBIOREV.2021.10.028.
12. Liu C, Wei H, Gong NJ, Cronin M, Dibb R, Decker K. Quantitative susceptibility mapping: contrast mechanisms and clinical applications. *Tomography*. 2015;1(1):3–17. doi:10.18383/j.tom.2015.00136.
13. Langkammer C, Liu T, Khalil M, *et al*. Quantitative susceptibility mapping in multiple sclerosis. *Radiology.* 2013;267(2):551–559. doi:10.1148/radiol.12120707.
14. Liu C, Li W, Tong KA, Yeom KW, Kuzminski S. Susceptibility-weighted imaging and quantitative susceptibility mapping in the brain. *J Magn Reson Imaging.* 2015;42(1):23–41. doi:10.1002/jmri.24768.
15. Wang Y, Liu T. Quantitative susceptibility mapping (QSM): Decoding MRI data for a tissue magnetic biomarker. *Magn Reson Med.* 2015;73(1):82–101. doi:10.1002/mrm.25358.
16. Ganz T, Nemeth E. Regulation of iron acquisition and iron distribution in mammals. *Biochim Biophys Acta.* 2006;1763(7):690–699. doi:10.1016/J.BBAMCR.2006.03.014.
17. Stankiewicz J, Panter SS, Neema M, Arora A, Batt CE, Bakshi R. Iron in chronic brain disorders: imaging and neurotherapeutic implications. *Neurotherapeutics*. 2007;4(3):371–386. doi:10.1016/J.NURT.2007.05.006.
18. Hare D, Ayton S, Bush A, Lei P. A delicate balance: Iron metabolism and diseases of the brain. *Front Aging Neurosci.* 2013;5(JUL):34. doi:10.3389/FNAGI.2013.00034.

19. Moos T, Morgan EH. The metabolism of neuronal iron and its pathogenic role in neurological disease: review. *Ann N Y Acad Sci.* 2004;1012:14–26. doi:10.1196/ANNALS.1306.002.
20. Xu M, Guo Y, Cheng J, *et al*. Brain iron assessment in patients with First-episode schizophrenia using quantitative susceptibility mapping. *Neuroimage Clin*. 2021;31:102736. doi:10.1016/J.NICL.2021.102736.
21. Francois C, Nguyen-Legros J, Percheron G. Topographical and cytological localization of iron in rat and monkey brains. *Brain Res.* 1981;215(1-2):317–322. doi:10.1016/0006-8993(81)90510-2.
22. Zheng W, Monnot AD. Regulation of brain iron and copper homeostasis by brain barrier systems: implication in neurodegenerative diseases. *Pharmacol Ther.* 2012;133(2):177–188. doi:10.1016/J.PHARMTHERA.2011.10.006.
23. Langkammer C, Pirpamer L, Seiler S, *et al*. Quantitative susceptibility mapping in parkinson's disease. *PLoS One.* 2016;11(9):1–13. doi:10.1371/JOURNAL.PONE.0162460.
24. Chen L, Hua J, Ross CA, Cai S, van Zijl PCM, Li X. Altered brain iron content and deposition rate in Huntington's disease as indicated by quantitative susceptibility MRI. *J Neurosci Res.* 2019;97(4):467–479. doi:10.1002/JNR.24358.
25. Kim SW, Stewart R, Park WY, *et al*. Latent iron deficiency as a marker of negative symptoms in patients with first-episode schizophrenia spectrum disorder. *Nutrients*. 2018;10(11):1–11. doi:10.3390/NU10111707.
26. Cuesta MJ, Lecumberri P, Moreno-Izco L, *et al*. Motor abnormalities and basal ganglia in first-episode psychosis (FEP). *Psychol Med.* 2021;51(10):1625–1636. doi:10.1017/S0033291720000343.
27. Langkammer C, Schweser F, Krebs N, *et al*. Quantitative susceptibility mapping (QSM) as a means to measure brain iron? A post mortem validation study. *Neuroimage.* 2012;62(3):1593–1599. doi:10.1016/j.neuroimage.2012.05.049.
28. Zucca FA, Segura-Aguilar J, Ferrari E, *et al*. Interactions of iron, dopamine and neuromelanin pathways in brain aging and Parkinson's disease. *Prog Neurobiol.* 2017;155:96–119. doi:10.1016/j.pneurobio.2015.09.012.
29. Isaias IU, Trujillo P, Summers P, *et al*. Neuromelanin imaging and dopaminergic loss in parkinson's disease. *Front Aging Neurosci.* 2016;8(AUG):196. doi:10.3389/fnagi.2016.00196.
30. Sheehan DV, Sheehan KH, Shytle RD, *et al*. Reliability and validity of the mini international neuropsychiatric interview for children and adolescents (MINI-KID). *J Clin Psychiatry.* 2010;71(3):313–326. doi:10.4088/JCP.09m05305whi.
31. Guías Clínicas AUGE Tratamiento de personas desde el primer episodio de Esquizofrenia. Departamento de Salud Mental. Ministerio de Salud; 2017. https://diprece.minsal.cl/wrdprss_minsal/wp-content/uploads/2017/07/GPC_EQZ.pdf
32. Opler MGA, Yavorsky C, Daniel DG. Positive and negative syndrome scale (panss) training: challenges, solutions, and future directions. *Innov Clin Neurosci*. 2017;14(11-12):77–81.
33. Power JD, Barnes KA, Snyder AZ, Schlaggar BL, Petersen SE. Spurious but systematic correlations in functional connectivity MRI networks arise from subject motion. *Neuroimage.* 2012;59(3):2142–2154. doi:10.1016/j.neuroimage.2011.10.018.
34. Power JD, Plitt M, Kundu P, Bandettini PA, Martin A. Temporal interpolation alters motion in fMRI scans: magnitudes and consequences for artifact detection. *PLoS One.* 2017;12(9):1–20. doi:10.1371/journal.pone.0182939.
35. Li W, Avram AV, Wu B, Xiao X, Liu C. Integrated Laplacian-based phase unwrapping and background phase removal for quantitative susceptibility mapping. *NMR Biomed.* 2014;27(2):219–227. doi:10.1002/nbm.3056.
36. Zhou D, Liu T, Spincemaille P, Wang Y. Background field removal by solving the Laplacian boundary value problem. *NMR Biomed.* 2014;27(3):312–319. doi:10.1002/nbm.3064.
37. Kan H, Arai N, Takizawa M, *et al*. Background field removal technique based on non-regularized variable kernels sophisticated harmonic artifact reduction for phase data for quantitative susceptibility mapping. *Magn Reson Imaging.* 2018;52:94–101. doi:10.1016/j.mri.2018.06.006.
38. Milovic C, Bilgic B, Zhao B, Acosta-Cabronero J, Tejos C. Fast nonlinear susceptibility inversion with variational regularization. *Magn Reson Med.* 2018;80(2):814–821. doi:10.1002/mrm.27073.
39. Milovic C, Bilgic B, Zhao B, Langkammer C, Tejos C, Acosta-Cabronero J. Weak-harmonic regularization for quantitative susceptibility mapping. *Magn Reson Med.* 2019;81(2):1399–1411. doi:10.1002/mrm.27483.
40. Chen DQ, Cheng LZ. Spatially adapted total variation model to remove multiplicative noise. *IEEE Trans Image Process.* 2012;21(4):1650–1662. doi:10.1109/TIP.2011.2172801.
41. Milovic C, Prieto C, Bilgic B, *et al*. Comparison of parameter optimization methods for quantitative susceptibility mapping. *Magn Reson Med.* 2021;85(1):480–494. doi:10.1002/MRM.28435.
42. Xiao Y, Fonov V, Bériault S, *et al*. Multi-contrast unbiased MRI atlas of a Parkinson's disease population. *Int J Comput Assist Radiol Surg*. 2015;10(3):329–341. doi:10.1007/s11548-014-1068-y.
43. Xiao Y, Beriault S, Pike GB, Collins DL. Multicontrast multiecho FLASH MRI for targeting the subthalamic nucleus. *Magn Reson Imaging.* 2012;30(5):627–640. doi:10.1016/j.mri.2012.02.006.
44. Xiao Y, Fonov V, Chakravarty MM, *et al*. A dataset of multi-contrast population-averaged brain MRI atlases of a Parkinson's disease cohort. *Data Brief*. 2017;12:370–379. doi:10.1016/j.dib.2017.04.013.
45. Cnaan A, Laird NM, Slasor P. Tutorial in biostatistics using the general linear mixed model to analyse unbalanced repeated measures and longitudinal data. *Stat Med.* 1997;16:2349–2380. doi:10.1002/(SICI)1097-0258(19971030)16:20<2349::AID-SIM667>3.0.CO;2-E.
46. Bates DM, Pinheiro JC. José C. Pinheiro mixcd-effects models in S and S-PLUS ö springer mixed-effects models in S and S-PLUS 4y springer contents. In: *Mixed-Effects Models in S and S-PLUS*. New York, NY: Springer; 2009.
47. Linear Mixed Models for Longitudinal Data. *Linear Mixed Models for Longitudinal Data*. Published online 2000. doi:10.1007/B98969
48. Liang KY, Zeger SL. Longitudinal data analysis using generalized linear models. *Biometrika*. 1986;73(1):13–22. doi:10.1093/BIOMET/73.1.13.
49. Halekoh U, Højsgaard S, Yan J. The R Package geepack for Generalized Estimating Equations. *J Stat Softw*. 2006;15(2):1–11. doi:10.18637/JSS.V015.I02.
50. Kim J, Wessling-Resnick M. Iron and mechanisms of emotional behavior. *J Nutr Biochem.* 2014;25(11):1101–1107. doi:10.1016/J.JNUTBIO.2014.07.003.
51. Egerton A, Chaddock CA, Winton-Brown TT, *et al*. Presynaptic striatal dopamine dysfunction in people at ultra-high risk for psychosis: findings in a second

cohort. *Biol Psychiatry.* 2013;74(2):106–112. doi:10.1016/J.BIOPSYCH.2012.11.017.

52. Fornito A, Harrison BJ, Goodby E, *et al*. Functional dysconnectivity of corticostriatal circuitry as a risk phenotype for psychosis. *JAMA Psychiatry*. 2013;70(11):1143–1151. doi:10.1001/JAMAPSYCHIATRY.2013.1976.
53. Perez-Costas E, Melendez-Ferro M, Roberts RC. Basal ganglia pathology in schizophrenia: dopamine connections and anomalies. *J Neurochem.* 2010;113(2):287287.–2872302. doi:10.1111/J.1471-4159.2010.06604.X.
54. Zecca L, Bellei C, Costi P, *et al*. New melanic pigments in the human brain that accumulate in aging and block environmental toxic metals. *Proc Natl Acad Sci U S A.* 2008;105(45):17567–17572. doi:10.1073/pnas.0808768105.
55. Cazorla M, deCarvalho FD, Chohan MO, *et al*. Dopamine D2 receptors regulate the anatomical balance of basal ganglia circuitry. *Neuron.* 2014;81(1):153. doi:10.1016/J.NEURON.2013.10.041.
56. Duyn J. MR Susceptibility Imaging. *J Magn Reson.* 2013;229:198–207. doi:10.1016/J.JMR.2012.11.013.
57. Rouault TA. Iron on the brain. *Nat Genet.* 2001;28(4):299–300. doi:10.1038/91036.
58. Taege Y, Hagemeier J, Bergsland N, *et al*. Assessment of mesoscopic properties of deep gray matter iron through a model-based simultaneous analysis of magnetic susceptibility and R2*—A pilot study in patients with multiple sclerosis and normal controls. *Neuroimage.* 2019;186:308–320. doi:10.1016/J.NEUROIMAGE.2018.11.011.
59. Milovic C, Tejos C, Acosta-Cabronero J, *et al*. The 2016 QSM Challenge: Lessons learned and considerations for a future challenge design. *Magn Reson Med.* 2020;84(3):1624–1637. doi:10.1002/MRM.28185.
60. Acosta-Cabronero J, Betts MJ, Cardenas-Blanco A, Yang S, Nestor PJ. In vivo MRI mapping of brain iron deposition across the adult lifespan. *J Neurosci.* 2016;36(2):364–374. doi:10.1523/JNEUROSCI.1907-15.2016.
61. Zhang Y, Wei H, Cronin MJ, He N, Yan F, Liu C. Longitudinal data for magnetic susceptibility of normative human brain development and aging over the lifespan. *Data Brief*. 2018;20:623–631. doi:10.1016/j.dib.2018.06.005.
62. Birkl C, Langkammer C, Sati P, Enzinger C, Fazekas F, Ropele S. Quantitative susceptibility mapping to assess cerebral vascular compliance. *AJNR Am. J. Neuroradiol.*. 2019;40(3):460–463. doi:10.3174/AJNR.A5933.
63. van Erp T, Hibar DP, Rasmussen JM, *et al*. Subcortical brain volume abnormalities in 2028 individuals with schizophrenia and 2540 healthy controls via the ENIGMA consortium. *Mol Psychiatry.* 2016;21(4):547–553. doi:10.1038/MP.2015.63.
64. Chopra S, Fornito A, Francey SM, *et al*. Differentiating the effect of antipsychotic medication and illness on brain volume reductions in first-episode psychosis: A Longitudinal, Randomised, Triple-blind, Placebo-controlled MRI Study. *Neuropsychopharmacology.* 2021;46(8):1494–1501. doi:10.1038/S41386-021-00980-0.
65. Tarcijonas G, Foran W, Haas GL, Luna B, Sarpal DK. Intrinsic connectivity of the globus pallidus: an uncharted marker of functional prognosis in people with first-episode schizophrenia. *Schizophr Bull.* 2020;46(1):184–192. doi:10.1093/SCHBUL/SBZ034.
66. Bilgic B, Pfefferbaum A, Rohlfing T, Sullivan EV, Adalsteinsson E. MRI estimates of brain iron concentration in normal aging using quantitative susceptibility mapping. *Neuroimage.* 2012;59(3):2625–2635. doi:10.1016/j.neuroimage.2011.08.077.
67. Ghadery C, Pirpamer L, Hofer E, *et al*. R2* mapping for brain iron: Associations with cognition in normal aging. *Neurobiol Aging.* 2015;36(2):925–932. doi:10.1016/j.neurobiolaging.2014.09.013.
68. Mizrahi R, Agid O, Borlido C, *et al*. Effects of antipsychotics on D3 receptors: a clinical PET study in first episode antipsychotic naive patients with schizophrenia using [11C]-(+)-PHNO. *Schizophr Res.* 2011;131(1-3):63–68. doi:10.1016/J.SCHRES.2011.05.005.
69. Smith Y, Villalba R. Striatal and extrastriatal dopamine in the basal ganglia: An overview of its anatomical organization in normal and Parkinsonian brains. *Mov Disord.* 2008;23(S3):S534–S547. doi:10.1002/MDS.22027.